The complex environment of the high excitation planetary nebula NGC 3242.

J. Meaburn,

University of Manchester, Jodrell Bank Observatory, Macclesfield, Cheshire, UK, SK11 9DL.

J. A. López,

Instituto de Astronomía, UNAM, Apdo. Postal 877, Ensenada, B.C. 22800, México.

A. Noriega-Crespo

Infrared Processing and Analysis Center - SIRTF Science Center, California Institute of Technology, Pasadena, California, 91125, USA

Received _____; accepted _____

Submitted AJ Sept 1st, 1999

ABSTRACT

Spatially resolved profiles of the Hα , [N II] 6584 Å and [O III] 5007 Å nebular emission lines, obtained with the Manchester echelle spectrometer combined with the 2.1 m San Pedro Mártir telescope have revealed the velocity structure of the nebular core and of one of the three (A, B and C) inner 'haloes' of the high excitation planetary nebula NGC 3242. The core is shown to have a cylindrical structure expanding at 25 km s^{-1}. The bright, diffuse, line emitting, inner spherical halo A surrounding the intensely bright elliptical core is shown to be limb brightened but its expansion velocity is unclear. The surrounding diffuse, 2.5 pc diam., halo B, is modelled by a thick shell expanding at 20 km s^{-1} although the contribution of scattered [O III] 5007 Å emission is unknown at present. The origin of the broad profiles from the fainter, patchy, 0.44 pc diam., halo C is again somewhat uncertain and may originate in scattered core light. FIR observations with IRAS and ISO reveal the presence of warm dust throughout the core and inner haloes on NGC 3242.

There is a large filamentary structure of line emitting gas 1.7 pc to the west of the nebular core. This is shown to be the western boundary of extended FIR emission from warm dust. A patchy component associated with this filamentary nebulosity emits the [O III] 5007 Å line with anomalous high intensity yet is shown here to be kinematically relatively inert. Likewise [N II] 6584 Å profiles from the filamentary edge are very narrow with turbulent motions of 8 km s^{-1}. Certainly the arc is being photoionized by leakage radiation from NGC 3242 but the radial velocities of the line profiles are inconsistent with its origin as a simple shell expanding radially from this PN. An assymetric lobe remains a possibility in which case the arc could be an ancient halo of NGC 3242.

Strange, faint, broad [O III] 5007 Å line profiles are found over the whole 15′

diameter area being considered here. The extended FIR emission region implies the presence of hot dust and suggests therefore that these [O III] 5007 Å line profiles could have a scattered origin.

Subject headings: Planetary nebulae: individual (NGC 3242)– kinematics and dynamics—haloes

1. Introduction

The diffuse and filamentary haloes of planetary nebulae (PNe) deserve particular attention for they trace the outflows that preceded the PN evolutionary phase. These often multiple haloes (e.g. Kaler, 1974, Pottasch, 1984, Chu et al, 1987) can take several distinctly different forms. For instance, the giant, spherical, outer halo around NGC 6543 has a dramatic filamentary appearance, emits the high excitation [O III] 5007 Å nebular line anomalously strongly, yet is kinematically, extraordinarily inert (Middlemas et al 1989, Bryce et al 1992a). Its overall expansion velocity is ≤ 7 km s^{-1}. The most likely explanation is that this giant halo is a relic of the slow, dense but very clumpy asymptotic giant branch (AGB) wind that preceded the formation of the PN. Incidentally, a high–excitation, giant, outer filamentary halo to the PN NGC 7009, with a similar appearance to that of NGC 6543, has just been discovered (Moreno-Corral et al 1998). Kinematical measurements are awaited.

Low–excitation strings of ionized knots forming the outer haloes of the PNe NGC 40 (Meaburn et al 1996) and IC 4593 (O'Connor et al 1999) also exhibit very low global expansion velocities. Yet the definite 15 km s^{-1} expansion velocity of the 130 arcsec diameter, more diffuse but limb brightened, spherical line emission outer halo of NGC 6826 was measured by Bryce et al (1992b). In this first unambiguous measurement of such an expansion velocity, an expanding, thick–shell model was developed to interpret the broadened, yet still single, line profiles. This thick shell approach has since been adopted by Guerrero et al (1998) and applied to several other diffuse PN haloes. In their interpretation, however scattered components to the halo line profiles were not considered.

The complication introduced by a possible scattered component to any line profile in measurements of such faint haloes was recognised by Pottasch (1984) and appreciated by Bryce et al (1992a & b) and Meaburn et al (1996). The problem arises because the inner

nebular cores emit the lines with surface brightnesses that are $\geq 10^4$ times greater than the diffuse haloes in their close proximity. A significant fraction of line emission from a bright core can scatter off halo dust and/or within the atmosphere and telescope optics to add to the intrinsic line emission from an ionized halo. Line profiles, with decreasing width as a function of halo radius, can safely be interpreted as being of predominantly intrinsic origin. However, spectropolarimetric measurements are really required to assess the scattered, polarised, fraction of a halo line profile.

In the present paper the environs of the PN, NGC 3242, are investigated. NGC 3242 has not only a three component (A, B and C) inner halo but potentially a huge, asymmetric filamentary halo as well. It is the latter structure that stimulated the present kinematical investigation with the prospect that this extensive feature is the relic of a very old, slow, dense, Red Giant wind emitted in the early AGB phase of the progenitor's evolution. Alternatively, the extensive filamentary halo could be simply ambient gas unrelated to the PN. With either origin it is likely that the filamentary gas is photoionized by the leakage of very hard photons from NGC 3242.

NGC 3242 is a high excitation planetary nebula (Class 7 Pottasch 1984) powered by a $\leq 1000\ L_\odot$ (Pottasch 1984) SD0 star (Heap 1986) with a surface temperature of T_{eff} = 60,000 K (Acker et al 1992). This implies that the present stellar mass is $\leq 0.45\ M_\odot$ with that of the progenitor $\approx 1\ M_\odot$ (Pottasch 1984).

At an 'expansion proper motion' distance to NGC 3242 of 0.47 Kpc (Terzian 1998) the linear scale at the nebula becomes 2.28×10^{-3} pc arcsec^{-1}. The central, elliptical shell is $\approx$ 21 arcsec across ($\equiv 4.8\ 10^{-2}$ pc - see the major axis in Fig 1(a)) and expanding at 25–30 km s^{-1} (Balick et al 1987). This shell is presumably generated by the fast wind (Kahn & West 1985, Mellema 1995) and is emitting intensely in the nebular emission lines. The bright, amorphous, 50.5 arcsec diameter ($\equiv$ 0.115 pc) spherical, limb-brightened, halo (A)

into which protrude two high–speed, lowly–ionized knots ('fliers') (Balick et al 1993, 1999 and Corradi et al 1996) can also be seen in Fig. 1(a). The surrounding, faint, diffuse (B) and patchy (C), haloes of 109 arcsec (≡ 0.25 pc) and 192 arcsec (≡ 0.44 pc) diameters respectively can be seen in Fig.1(b).

The extended filamentary arc (Deeming 1966) of particular interest here, is (see the POSS print in Fig. 1(c)) 12.5 arcmin (≡ 1.7 pc) to the West of the bright nebular core and possibly associated with NGC 3242 (Zanin & Weinberger 1997). Certainly their measurement of its [O III] 5007 Å /Hα intensity ratio of 5, which is very similar to that of the giant filamentary halo of NGC 6543, indicates an unusual origin. This ratio is both higher than 3 measured by Perinotto et al (1994) for the core of NGC 3242 and far higher than can be produced by photoionized gas with reasonable abundances. Incidentally, additional heating by a low mach shock, produced by a mass-loaded wind, was invoked to explain the same high ratio in the NGC 6543 halo (Meaburn et al 1991).

The profiles of the Hα , [N II] 6584 Å & [O III] 5007 Å nebular emission lines of the core, the central haloes of NGC 3242, as well as those of this large filamentary arc, were obtained with the Manchester echelle spectrometer (MES) with the hope that the origin and nature of these various structures would become clarified with a proper appreciation of their kinematics. However, it was during these observations that a fourth distinctly separate and unexpected component was discovered. Broad, but faint, [O III] 5007 Å line profiles were found from a diffuse region encompassing the whole area being considered i.e ± 15′ (i.e. ± 2 pc) from NGC 3242. Consequently, this emission was also investigated with MES. Its presence prompted a parallel search for IRAS and ISO FIR emission characteristic of hot dust which could be scattering the optical line emission from the nebular core. The consequences of both of these further observations are also presented here.

2. Observations and results

2.1. Optical imagery

The images in Fig. 1(a& b) were obtained with the 2.1 m SPM reflecting telescope through a 50Å bandwidth interference filter centred on the Hα and [O III] 5007 Å emission lines respectively. The detector was the Thomson CCD with pixel sizes $\equiv 0.246 \times 0.246$ arcsec^2 to give a field size of 4×4 arcmin^2.

The bright elliptical core of NGC 3242 can be seen in the contour map plus greyscale in Fig. 1(a) surrounded by the bright spherical halo (A). The fainter, outer, spherical halo (B) is apparent in the deeper print in Fig. 1(b). The patchy features tin Fig. 1(b) that constitute halo (B) in the vicinity of such a bright central source could be optical ghosts. However, their reality is assured for they are present in two images with completely separate origins i.e. one with the SPM 0.6 m diameter telescope and in a deep print of the red POSSII plate.

The image of the adjacent, giant filamentary arc in Fig. 1(c) is from the POSSII red plate with co-ordinates superimposed using the Starlink GAIA software package.

2.2. Echelle spectrometry

Spatially resolved, longslit line profiles at high spectral resolution were obtained in April 1995 and March 1997 with the MES (Meaburn et al 1984) combined with the f/7.9 focus of the 2.1m San Pedro Mártir UNAM telescope. This spectrometer has no cross-dispersion. For the present observations, a filter of 90 Å bandwidth was used to isolate the 87th order containing the Hα and [N II] 6584 Å nebular emission lines and 70 Å bandwidth the 114th order containing [O III] 5007 Å .

A Textronik CCD with 1024 × 1024, 24 μm, square pixels was the detector. Two times binning was employed in the spatial dimension. Consequently 512 increments, each 0.60″ long, gave a total projected slit length of 5′.12 on the sky. 'Seeing' varied between 1-2″ during these observations.

Either a 70 μm wide ($\equiv$ 5 km s^{-1} and 1″) 5-element multi-slit or a 150 μm wide ($\equiv$ 10 km s^{-1} and 1.9″) single slit was used. These slit lengths were always orientated EW.

The data were bias corrected, cleaned etc. in the usual way using the Starlink Figaro and Kappa software packages. All spectra were calibrated in wavelength to $\pm$ 1 km s^{-1} accuracy against spectra of a thorium/argon lamp.

Position 2, of a single slit through the nebular core where an [O III] 5007 Å 60 sec integration was obtained is shown in Fig. 1(b). The resultant contour map (with log intervals) combined with a greyscale image of part of this position/velocity (pv) array is shown in Fig. 2(a). The [O III] 5007 Å line profile from the centre of this array (arrowed in Fig. 1(b)) is shown in Fig. 2(b). It can be seen that [O III] 5007 Å splits into two velocity components over the nebular centre i.e. at V_{hel} = -15 and +24 km s^{-1}. The systemic heliocentric radial velocity V_{sys} = 9 km s^{-1} is given by the central minimum in Fig. 2(a). The approaching and receding wings to the profile in Fig. 2(b) could be from the bright halo A in Fig. 1(a).

Two of the slit positions for one [O III] 5007 Å 1800 sec integration with the 5-element multi-slit are marked 1 and 3 in Fig. 1(b) against an image of NGC 3242. The resulting log contour/greyscale representations of the pv arrays of [O III] 5007 Å profiles are shown in Figs. 3(a & b) respectively. Both the atomic recombination continuum spectrum and that of a diffuse [O III] 5007 Å component over the whole slit length have been subtracted from these pv arrays. These slit positions cut the northern and southern edges of halo A to give the bright centres to the pv arrays. They also reveal the [O III] 5007 Å profiles from halo

B in the elliptical distribution in the two pv arrays about V_{sys}. The 'spike' to V_{hel} = 100 km s^{-1} in Fig. 3(b) is from the vicinity of the southern 'FLIER' in halo B.

A further slit position (not shown here) from the same 5-element multi-slit array crosses the southern 'patch' in halo C (see Fig. 1(b)). [O III] 5007 Å profiles from this are very flat-topped, 39 km s^{-1} wide and centred on V_{sys} of the core of NGC 3242.

Examples of the faint, broad [O III] 5007 Å profiles found in the vicinity of NGC 3242 are shown in the pv array in Fig. 4(a) from an 1800 s integration for Slit 4 (see Fig. 1(c)). The profile in Fig. 4(b) is for the coaddition of all of the [O III] 5007 Å profiles between 1′ to 3′ in Fig. 4(a). Two distinctly separate velocity components can be seen in this diffuse [O III] 5007 Å emission i.e. at V_{hel} = -3 and +20 km s^{-1}. This faint, diffuse [O III] 5007 Å feature, has been traced out ± 21.5′ both to the east and west of the nebular core (slit positions not shown here). It diminishes in brightness with distance from NGC 3242 but maintains its width over this range.

The single slit position, 5, where Hα , [N II] 6584 Å and [O III] 5007 Å profiles were obtained with 1800 s integrations from the outer filamentary shell is marked against the image in Fig. 1(c). Greyscale representations of the resultant pv arrays are shown in Figs. 5(a–c) respectively. The bright, narrow, Hα and [N II] 6584 Å profiles from this filamentary nebulosity are particularly striking. The faint, broad [O III] 5007 Å profiles found over the whole region are also clearly present in Fig. 5(c). However, the extended, patchy (to the east) narrow [O III] 5007 Å component from the filamentary arc appears to have an Hα and [N II] 6584 Å emitting sharp westward edge.

The Hα and [N II] 6584 Å profiles in Figs. 6(a & b) respectively are from the position arrowed in Fig. 5(b) over a filamentary edge. The profiles of the broad diffuse emission have been subtracted. The [N II] 6584 Å profile is particularly narrow (0.30 ± 0.3 Å HPBW) when compared with the width of the instrumental profile of 0.24Å (≡ 11 km s^{-1}).

The [O III] 5007 Å profile in Fig. 6(c) is for the emission from the patchy gas (between 0.34′ to 3.4′ along Slit 5) associated with the filamentary arc again with the profiles of the general diffuse component (between 4.1′ to 5.0′) subtracted (see Fig. 5(c). All of the Hα [N II] 6584 Å and [O III] 5007 Å profiles originating in the filamentary arc appear to be centred on $V_{hel} \approx 24$ km s^{-1} which is significantly displaced from $V_{sys} = 9$ km s^{-1} for the bright core of NGC 3242 (see Fig. 2(a)). Only the [O III] 5007 Å profiles in Fig. 6(c) have a minor component centred on $V_{hel} = -5$ km s^{-1}.

2.3. FIR mapping

The IRAS data in its 4 bands, 12, 25, 60 and 100μm can be used in two different but complementary ways by using both 'excess maps' and HiRes images. The excess maps are meant to show the distribution of gas and dust around a source based on their emission above the background. The background is estimated from the 100μm emission, where cirrus contamination is higher (see Van Buren et al. 1995). The data for the excess maps comes from the IRAS Sky Survey Atlas with 2°×2° fields at the four IRAS bands and a pixel size of 1.′5. The main limitation therefore of an excess map is its relatively low spatial resolution of a few arcminutes.

A slighly higher spatial resolution, to study smaller scales, can be achieved with the IRAS HiRes images. These images are based on data sample with a 15″ pixel scale and can reach down to ∼1′ spatial resolution. The HiRes images are created by applying an iterative procedure based on a 'maximum correlation' algorithm (Aumann et al. 1990; Cao et al. 1996; Noriega-Crespo et al . 1997ab). There are at least two things to keep in mind with the HiRes maps; one is the possibility of spurious features that arise during the iteration process, and second, that the background is not subtracted from the images.

A comparison of the POSSII image (greyscale) and the IRAS excess map at 60μm (contours) in a one degree field is shown in Fig. 7(a). The 'excess emission' extends to 15$'$ from the central object, and almost concides with the outer edge with the giant filamentary shell. In other objects, like runaway OB or Mira stars, shells or extended emission at 60μm are observed and interpreted as originating in warm dust at $T_{dust} \sim 40$ K (see e.g. Young et al. 1993; Raga et al. 1997). This may be also the case for NGC 3242 (see below).

The HiRes images can be used to check the presence of extended structure. Indeed a comparison of the same field in Fig. 7(b) confirms this extended feature but this time with a HiRes image at 25μm (contours). The image, despite the typical IRAS artifacts from the image reconstruction process, shows extended emission towards the SW that reaches beyond 10$'$ and near the edge of the giant optical filamentary arc. So the FIR extended emission is quite real.

The 60μm flux can be used to determine the mass of the extended emission region (Young et al. 1993), i. e.,

$$M_{extd} = \frac{F_{60}\ D^2\ \lambda^2\ \frac{4}{3}\ a\ \rho\ f}{B(\nu,T)\ Q(\nu)}, \tag{1}$$

where F_{60} is the 60μm flux, D is the distance to the source, a the size of the dust grain, ρ the dust density, $f = M_{gas}/M_{dust}$ (the gas to dust ratio), $B(\nu,T)$ the Planck function at frequency ν and temperature T, and $Q(\nu)$ is the dust emissivity. Using $a = 0.1\mu$m, $\rho = 3$ g cm^{-3}, Q(60μm) = 0.0046 (Draine & Lee 1984; Draine 1987), and assuming $f = 100$, and $T = 40$ K; eqn (1) can be written as:

$$M_{extd} = 0.03 M_{\odot} \left(\frac{F_{60}}{100\ \mathrm{Jy}}\right) \left(\frac{D}{200\ \mathrm{pc}}\right)^2. \tag{2}$$

The central flux at 60μm, within 5′ in the ISSA IRAS image, is $\sim$ 63 Jy, while the total flux within 8′ is $\sim$ 73 Jy; so for F_{60} = 10 Jy and D = 470 pc, this corresponds to $M_{extd} \sim 0.02 M_{\odot}$.

The question of the warm dust in the core of NGC 3242 is better illustrated perhaps by the spectrum (Fig. 7(c)) taken with ISO Long Wavelength Spectrometer (LWS). Here the LWS spectrum was reduced and analyzed using the interactive LWS package LIA and the ISO Spectral Analysis Package (ISAP V1.6). The spectrum displays the well known and very strong [O III] 51.8μm and 88.3μm lines (Dinerstein et al. 1985), as well as the [N III] 57.3μm line. The spectrum is not flat, but lies over a continuum which can be modeled as black body with a temperature of 46 K. The fit is so good (Fig. 7(c), dotted line) that it merges into the data. The LWS aperture is $\sim$ 90″ and so the spectrum is for the whole of the innermost region of the nebula, nevertheless it suggests that the presence of warm dust at large distances from the core is quite possible.

It is interesting to notice from the LWS spectrum that the intensity ratio of the [O III] lines 52.8 to 88.5μm is 2.1, i.e. lower than that obtained by Dinerstein et al. 1985, which implies a lower electron density (log n_e = 2.5). Finally, a consistency check on the ISO photometry can be performed by comparing the LWS spectrum (convolved with IRAS bandpasses which fall within its wavelength range) with the IRAS measurements. Using the ISAP photometric package, we obtain $F_{lws,60}$ = 50 Jy and $F_{lws,100}$ = 33 Jy, compared with $F_{iras,60}$ = 53$\pm$14 Jy , and $F_{iras,100}$ = 29$\pm$13 Jy, i.e. in very good agreement.

3. Morphology and kinematics

3.1. The core

The contour map in Fig. 1(a) suggests that the dominant part of the [O III] 5007 Å emitting region of the nebular core is composed of a cylindrical structure whose axis lies along PA56°. If this cylinder has a circular section then to produce the degree of ellipticity (i.e. major/minor axis ratio of 1.26) the cylinder axis must be tilted at 52.6° to the plane of the sky. The brightest velocity components in the pv array in Fig. 2(a) within this simple model suggests that the south west edge of the cylinder is nearest the observer i.e. it has an approaching radial velocity compared to V_{sys}. As the brightest velocity components in Fig. 2(a) are separated in radial velocity by 30 km s^{-1} then the expansion velocity of the cylinder, assumed to be perpendicular to its axis, is $V_{exp} = 30/(2 \cos 52.6°) = 25$ km s^{-1}. No doubt the nebular core has some sort of ellipsoidal structure along the axis of the cylinder. The best estimation of the morphology and kinematics of the core are shown in Fig. 8.

3.2. Haloes A, B and C

Little can be said about the kinematics of Halo A from the present spectral observations for these are so dominated by the motions of the bright core and associated phenomena in this vicinity (e.g. FLIERS). It is notable that in Fig. 1(a) Halo A is limb-brightened i.e. a bright ring defines the interface between Haloes A & B.

However, the parts of the pv arrays of [O III] 5007 Å profiles in Figs. 3(a & b) that cover Halo B (away from the array centres) suggest the presence of a thick, line emitting, expanding shell. The contours systematically change from around 50 km s^{-1} wide near their centres (either side of the bright northerly and southerly edges of Halo A) to 20 km s^{-1}

wide at their edges.

It is interesting to compare the predicted pv arrays of line profiles in Fig. 8(a) with the observed ones in Figs. 3(a & b). Here Halo B has been modelled in isolation by a spherical, thick shell, expanding uniformly at 20 km s^{-1} with inner and outer radii of 0.058 and 0.125 pc respectively to match the dimensions in Figs. 1 (a & b). The volume emissivity of the [O III] 5007 Å line, $\epsilon_{[O\ III]\ 5007\ \mathring{A}}$ (erg cm^{-3}), can be shown to decline as radius^{-4} as would be expected for an ionized particle wind which has a constant mass loss rate over the period of formation of Shell B (see Meaburn 1988 and Bryce, Meaburn & Walsh 1992b for model background).

For an ionized hydrogen particle wind of velocity V km s^{-1} with a mass-loss-rate $\dot{M}$ solar masses yr^{-1} then at radius R pc from the star the atomic hydrogen number density is given by

$$n(R) = 3.35 \times 10^6 \dot{M} R^{-2} V^{-1}\ \mathrm{cm}^{-3} \qquad (3).$$

If this wind is completely ionized, of uniform electron temperature (say $T_e \approx 10^4$ K) and the small fraction of oxygen present is in the doubly ionized state then the volume emissivity of [O III] 5007 Å emission is given by

$$\epsilon_{[O\ III]\ 5007\ \mathring{A}} \propto n(R)^2 \propto R^{-4} \qquad (4).$$

In the present model, all of the predicted [O III] 5007 Å line profiles from this thick shell model have been convolved with a Gaussian of 20 km s^{-1} width (i.e the observed [O III] 5007 Å profile width at the halo circumference) to account for internal turbulence within the thick shell, instrumental broadening etc. The pv array in Fig. 9(a) is for a slit over the centre of the shell. The observed tapering in profile widths from the edges of Halo

A to B is predicted convincingly by this simple model. Furthermore, it is interesting that a brightness peak at a radius of 0.058 pc occurs on the interface of Shells A & B. This is illustrated in Fig. 9(b) where the relative surface brightnesses of [O III] 5007 Å profiles from the model, integrated over their spectral widths, are plotted against radius.

A strong reservation about the straightforward acceptance of the reality of this line emitting model for Halo B is posed by the certainty (see Sect. 2.2) that this halo also contains significant amounts of dust. With a core/Halo B [O III] 5007 Å brightness ratio of ≈ 780 then significant Mie scattering of the core profiles could be mixed with any of intrinsic origin. Spectropolarimetry of the [O III] 5007 Å profiles is awaited to assess the magnitude of this complication. The good match of the observed and model profiles suggests that scattering is not dominant in Halo B. Such scattering is a plausible explanation of 39 km s^{-1} wide [O III] 5007 Å profiles from halo C (Sect. 2.2). There is no sign of a systematic expansion of the latter halo in the present data.

3.3. The giant diffuse and filamentary regions

The interpretation of the diffuse, broad component of [O III] 5007 Å (see Figs. 4(a & b)) found up to 15′ (2 pc) from NGC 3242 poses problems. Its velocity profile is narrower but somewhat similar to that of the bright nebular core (see Figs. 2(a & b)) and even at a distance of only 2′ from the core it is 8000 times fainter. Its width does not diminish with distance from NGC 3242 as would be expected for a radially expanding shell. Scattering of the intense core [O III] 5007 Å emission by the diffuse, ambient, FIR emitting, interstellar dust (or even the Earth's atmosphere) is immediately suggested.

This possibility is made less certain by the Hα , [N II] 6584 Å & [O III] 5007 Å profiles (Figs. 5(a–c) and 6(a–c) from the filamentary nebulosity Fig. 1(c)) 1.7 pc to the West of

NGC 3242. These profiles are all narrow and their brightest peaks are centred on V_{hel} = 24 km s^{-1} which is significantly displaced from V_{sys} = 9 km s^{-1} of NGC 3242 and coincident with the receding velocity component of the diffuse [O III] 5007 Å emission. Undoubtably, line emitting gas is being observed which is photoionized by the leakage of Lyman photons from NGC 3242. The localised region emitting a very narrow [N II] 6584 Å line (arrowed in Fig. 5(b)) must be the bright rim behind an ionization front, viewed tangentially and moving into a neutral cloud (to the West).

Firstly, it would be interesting to estimate the electron temperature, T_e, and turbulent motions, δV_{turb}, within the arrowed filament using the relative widths of the Hα and [N II] 6584 Å profiles in Figs. 5(a & b). This method is usually applicable to situations, as here, where the [N II] 6584 Å profiles are exceptionally narrow because of low turbulent motions; and has been successfully applied to the inert haloes of the PNe, NGC 6543, NGC 40 and IC 4593 (Meaburn et al 1991 & 1996 and O'Connor et al 1999 respectively). Unexceptional values of $T_e \approx 10^4$K were found in these haloes by this method. However, simple inspection of the assymetric Hα profile in Fig. 6(a) suggests that there is significantly more turbulence within the Hα emitting volume than within the [N II] 6584 Å emitting one along the same sight line passing through this sharp filamentary edge. Maybe flows of a few tens of km s^{-1} down the pressure gradient, away from the ionization front, are being detected in the Hα profiles which do not occur in the [N II] 6584 Å emitting gas closer to the neutral gas. Consequently, any estimations of T_e from the profile widths would be most unreliable for the method depends critically on equal turbulence in both zones. If the observed velocity width of the [N II] 6584 Å profile in Fig. 6(b) is simulated by a Gaussian of halfwidth δV_{obs} then

$$\delta V_{turb} = (\delta V_{obs}^2 - \delta V_{inst}^2 - \delta V_{th}^2)^{1/2} \qquad (5),$$

where δV_{inst} is the instrumental halfwidth (11 km s^{-1}) and δV_{th} the thermal one (for T_e = 10^4 K) again simulated by Gaussians. In which case, for δV_{obs} = 13.6 km s^{-1} ($\equiv$ 0.30Å) then δV_{turb} = 8 $\pm$ 3 km s^{-1} for the [N II] 6584 Å emitting volume of the filament. These low turbulent motions at $\approx$ the sound speed in the ambient gas confirm the photoionized 'bright-rim' interpretation of the filamentary structure. For instance, an old, shocked, supernova filament would be emitting [N II] 6584 Å profiles broadened by many tens of km s^{-1}.

This [N II] 6584 Å filament then surrounds the more extended (2.5′ wide), again photionized, patchy [O III] 5007 Å emitting region (Fig. 5(c)), towards NGC 3242. The [O III] 5007 Å profile from this more extended emitting region (Fig. 6(c)) associated with the giant filamentary arc also has an enhanced velocity component at V_{hel} = -5 km s^{-1} which is coincident with the approaching component (Fig. 4(b)) of the faint diffuse emission. This result favours photoionization of the general diffuse gas as well as that of the patchy and filamentary components of the giant filamentary arc to give [O III] 5007 Å emission from all with but with [O III] 5007 Å scattering unimportant.

One strange aspect of all of the profiles shown here is that the receding velocity components of i) the bright core (Fig. 2(b)), ii) of the diffuse [O III] 5007 Å (Fig. 4(b)), iii) the patchy [O III] 5007 Å associated with the filamentary arc (Fig. 6(c)) and iv) both the Hα and [N II] 6584 Å emission from the filamentary edge of the arc (Figs. 6(a & b) are all centred on $V_{hel} \approx$ 24 km s^{-1} to be compared with V_{sys} = 9 km s^{-1} for NGC 3242 itself. If the giant arc was the filamentary edge, viewed tangentially, of a simple radially expanding shell centred on NGC 3242 then single line profiles on V_{sys} = 9 km s^{-1} would be expected. The only possibility then is that if this arc has an NGC 3242 origin it is the edge of an assymetric, irregular, single lobe. The outflow velocity would therefore be greater than the radial velocity difference 25 km s^{-1} - V_{sys} = 16 km s^{-1} measured here.

The extended ridge of FIR emission (Figs. 7(a & b)), which has the giant filamentary arc as its western boundary, is black-body emission from the heated dust also contained within this volume. The presence of this FIR ridge itself helps to directly associate the filamentary arc with NGC 3242.

4. Conclusions

The nebular core has a 'waisted' cylindrical structure expanding at 25 km s^{-1} away from this axis to give a kinematical age of 913 yrs to reach its present 0.048 pc diameter. There is direct evidence that the diffuse halo B, diam. 0.25 pc, surrounding the core is a thick shell expanding at $\approx$ 20 km s^{-1} to give a kinematical age of 5950 yrs.

The present optical results are inconclusive about the origin of the giant filamentary arc. The high [O III] 5007 Å /Hα brightness ratio, for its patchy component but not its filamentary edges, suggests highly processed material unlike the ambient ISM (see Sect. 1). The arc certainly seems to be photoinized by leakage radiation from NGC 3242 yet the bright velocity component in its line profiles are displaced by 16 km s^{-1} from V_{sys} of NGC 3242. If the arc is the edge of a lobe, expanding assymetrically from NGC 3242, then its kinematical age will be $\leq 10^5$ yrs for a radius of 1.7 pc. This timescale would place its origin firmly into the AGB phase of the projenitor's evolution.

IRAS and ISO observations indicate the presence of dust in all the regions considered here. The FIR ridge from the nebular core seems to confirm the NGC 3242 origin of the giant filamentary arc.

Acknowledgements

We wish to thank the staff of the San Pedro Mártir observatory for their excellent

assistance during these observations. JM is grateful to PPARC for funding the conversion of the Manchester echelle spectrometer for use on the San Pedro Mártir telescope. JAL acknowledges continuos support from CONACYT and DGAPA-UNAM. JM acknowledges the hospitality of IAUNAM – Ensenada where this paper was written and a grant from the Royal Society that funded this visit.

REFERENCES

Acker, A., Ochsenbein, F., Stenholm, B., Tylenda, R., Marcout, J. & Schohn, C., 1992, Strasbourg–ESO Catalogue of Galactic Planetary Nebulae (Garching:ESO).

Aumann, H.H., Fowler, J.W. & Melnyk, M. 1990, AJ, 99, 1674.

Balick, B., Rugers, M., Terzian & Chengalur, J. N., 1993, ApJ, 411, 778.

Balick, B., Preston,. H. L. & Icke, V., 1987, AJ, 94, 1641.

Balick, B., Hajian, A. R., Terzian, Y., Perinetto, M. & Patriarchi P., 1999, ApJ,,.

Bryce, M., Meaburn, J., Walsh, J. R. & Clegg, R. E. S., 1992a, MNRAS, 254, 477.

Bryce, M., Meaburn, J. & Walsh, J. R., 1992b, MNRAS, 259, 629.

Cao, Y., Prince, T.A., Terebey, S., Beichman, C.A. 1996, PASP, 108, 535.

Chu, Y–H, Jacoby, G. H. & Arendt, R., 1987, ApJ Suppl., 64, 529.

Corradi, R. L. M., Manso, R., Mampaso, A., Schwarz, H. E., 1996, Astron. Astr, 313, 913.

Deeming 1966 ApJ., 146, 287.

Dinerstein, H.L., Lester, D.F., & Werner, M.W. 1985, ApJ, 291, 561.

Draine, B., 1987, unpublished supplemet to Draine & Lee (1984).

Draine, B., & Lee, H.M. 1984, ApJ, 285, 89.

Guerrero, M. A., Villaver, E. & Manchado, A., 1998, ApJ, 507.

Heap, S. R., 1986, in 'Insights in Astrophysics', Proc. Joint NASA/ESA/SERC Conf., ESA SP, 263, 291.

Kahn, F. D. & West, K. A., 1985, MNRAS, 212, 837.

Kaler, J. B., 1974, AJ,79, 594.

Meaburn, J., 1988, MNRAS, 235, 375.

Meaburn, J., Blundell, B., Carling, R., Gregory, D. E., Keir, D. F. & Wynne, C. G., 1984, MNRAS, 210, 463.

Meaburn, J., Nicholson, R., Bryce, M., Dyson, J. E. & Walsh, J. R., 1991 MNRAS, 252, 535.

Meaburn, J., López, J. A., Bryce, M. & Mellema, G., 1996, Astron. Astr., 307, 579.

Mellema, G., 1995, MNRAS, 277, 173.

Middlemass, D., Clegg, R. E. S. & Walsh, J. R., 1989, MNRAS, 239,1.

Moreno–Corral, M. A., de la Fuente, E. & Gutiérrez, F., 1998, Revista Mex. Astr. Astr., 34, 117.

Noriega-Crespo, A., Van Buren, D., & Dgani, R. 1997a, AJ, 113, 780.

Noriega-Crespo, A., Van Buren, D., Cao, Y., & Dgani, R. 1997b, AJ, 114, 837.

O'Connor J. A., Meaburn, J., López, J. A., Redman, M. P. 1999, Astron. Astr., 346, 237.

Perinotto et al 1966, ApJ Suppl., 107, 481.

Pottasch, S. R., 1984, 'Planetary Nebulae' ASS library, Reidel.

Raga, A.C., Noriega-Crespo, A., Cantó, J., Steffen, W., Van Buren, D., Mellema, G., & Lundqvist, P. 1997, RMxAA, 33, 73.

Young, K., Phillips, T.G., & Knapp, G.R. 1993, ApJ, 409, 725.

Zanin, C. & Weinberger, R., 1997, IAU Symp. 180, 'Planetary Nebulae' eds Habing H. J. & Lamers, H. J. G. L. M., Kluwer Academic Publishers.

This manuscript was prepared with the AAS LaTeX macros v4.0.

Fig. 1.— a) An Hα contour map with evenly spaced $\log_{10}$ intervals, combined with a greyscale image of the core of NGC 3242. The highest contour is for $\log_{10} = 3.4$ (counts pixel^{-1}). The limb-brightened bright halo A is apparent. Also marked is the position angle of the axis of the cylinder of strong emission which most likely simulates the central structure. b) A deep negative greyscale representation of the [O III] 5007 Å image reveals the faint circular halo B and patchy halo C. The white square delineates the area covered by Fig. 1(a). Three EW slit positions, 1-3, are also marked. c) An image of the POSSII red plate reveals the large filamentary arc to the west of NGC 3242. Two EW slit positions, 4 & 5, are shown.

Fig. 2.— a) A contour map with evenly spaced $\log_{10}$ intervals of the position/velocity array of [O III] 5007 Å profiles along Slit 2 is shown combined with a greyscale representation of the same data array. This slit position crosses the central star of NGC 3242. The contours are from $\log_{10} = 0.3$ to 2.7 counts pixel^{-1}. b) The profile of the [O III] 5007 Å line for the position arrowed in Fig. 2(a).

Fig. 3.— a) A contour/greyscale map with evenly spaced $\log_{10}$ intervals (from 0.3 to 2.7) of the position/velocity array of [O III] 5007 Å profiles along Slit 1. The continuum spectrum and that of the diffuse broad [O III] 5007 Å component along the whole slit length have both been removed. b) As for a) but for $\log_{10}$ contour intervals between 0.8 to 4.0.

Fig. 4.— A deep negative greyscale representation of the position/velocity array of [O III] 5007 Å profiles along Slit 4, to the east of NGC 3242. b) The [O III] 5007 Å line profile for all of the data between 1′ - 3′ in Fig. 4(a) coadded.

Fig. 5.— The negative greyscale representations of the a) Hα , b) [N II] 6584 Å & c) [O III] 5007 Å line profiles along the position/velocity arrays for Slit 5. This slit position crosses the giant filamentary arc to the west of NGC 3242.

Fig. 6.— The observed a) Hα and b) [N II] 6584 Å line profiles for the sharp filament (arrowed in Fig. 5(b)). c) The [O III] 5007 Å integrated line profile for 0.34′ to 3.4′ along Slit 5 (see Fig. 5(c)). The diffuse background component derived from the westerly end of the slit has been subtracted.

Fig. 7.— a) A comparison of the Palomar Survey image of NGC 3242 over a 1° field (greyscale) and an IRAS excess map at 60μm characteristic of warm dust emission (contours). b) The same field, but this time the contours correspond to an IRAS HiRes image at 25μm with a $\sim$ 1′ spatial resolution. c) The ISO LWS spectrum of the core of NCG 3242 showing the very strong [O III] 51.81 and 88.35μm lines, as well as the [N III] 57.33μm line. The bottom panel is an enlargement to show the continuum and the black body fit with T = 46 K (dotted line).

Fig. 8.— A schematic model of the bright core (see Figs. 1(a) and 2(a)) of NGC 3242. Here a central cylinder with circular section (shaded) and V_{exp} = 25 km s^{-1} has a high volume emissivity of the [O III] 5007 Å line. This, when viewed by the observer, has its axis along PA56° and inclined at 52.6° to the plane of the sky. The south–westerly edge of the cylinder is nearest the observer to give the approaching radial velocity shifts that are observed. The ellipsoidal shape of the rest of the core is hypothetical.

Fig. 9.— a) A contour map with linear intervals of a predicted position/velocity array crossing the centre of a spherical, radially expanding (V_{exp} = 20 km s^{-1}) thick shell of [O III] 5007 Å emitting gas is shown. The volume emissivity of the [O III] 5007 Å line is assumed to fall off as radius^{-4} similar to emission from an ionized stellar particle wind whose ejection is temporally invariable and with no ionisation stratification. Some of the observed characteristics of the longslit spectra of Halo B are simulated. b) The relative variation (counts) in surface brightness of the position/velocity array in a) integrated over the whole velocity range of the [O III] 5007 Å profiles.

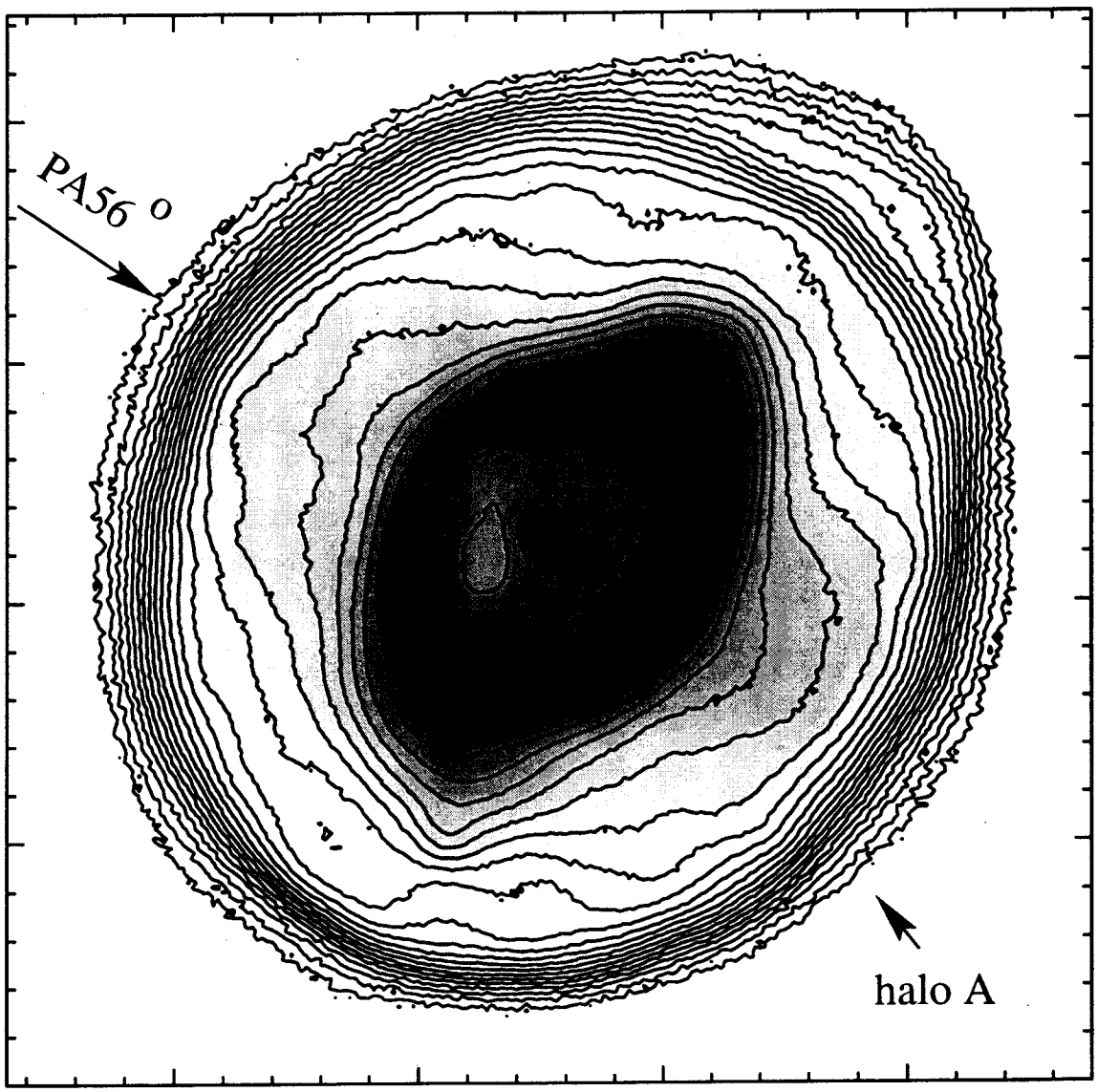

30 arcsec

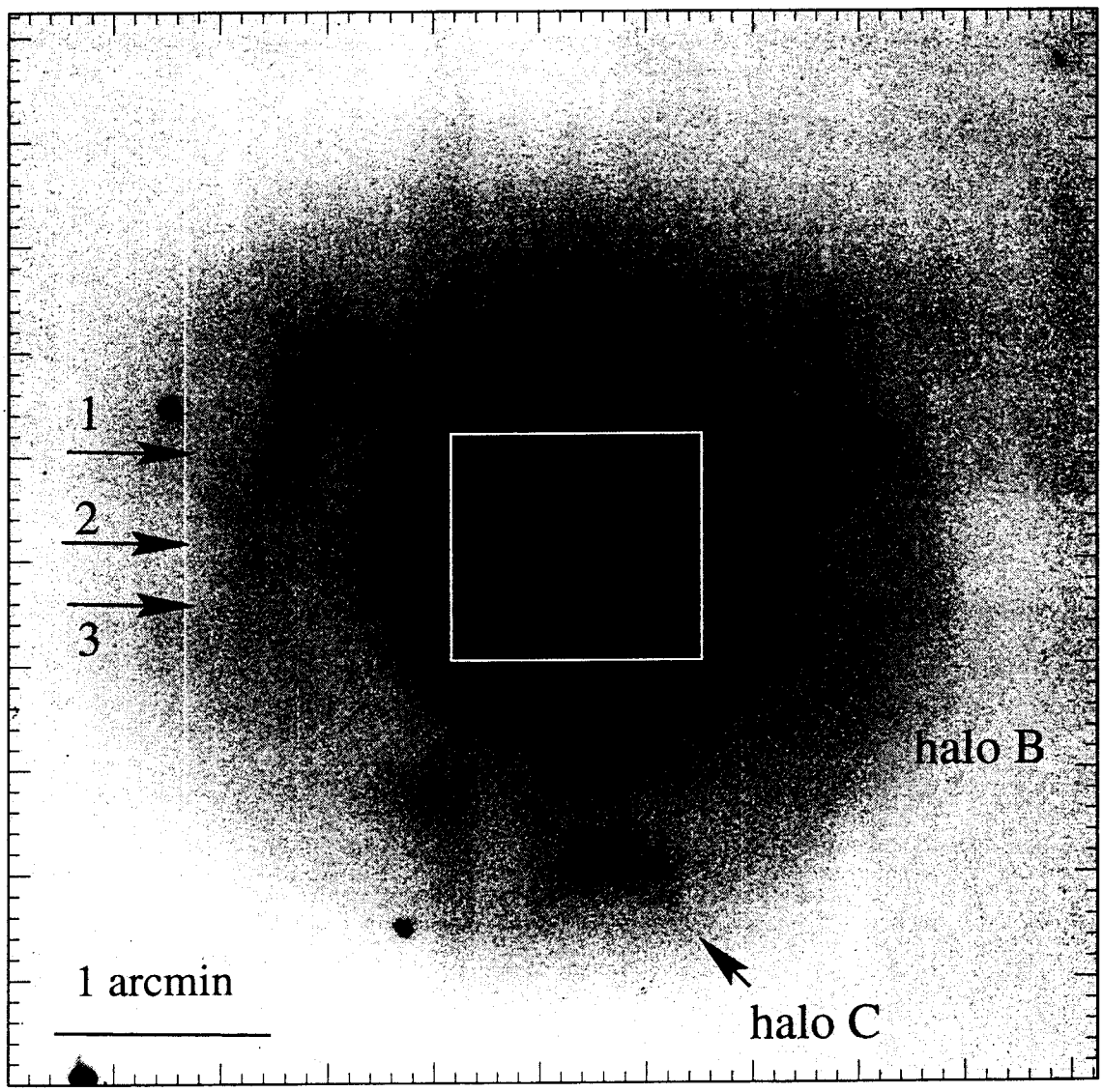
1
2
3
halo B
1 arcmin
halo C

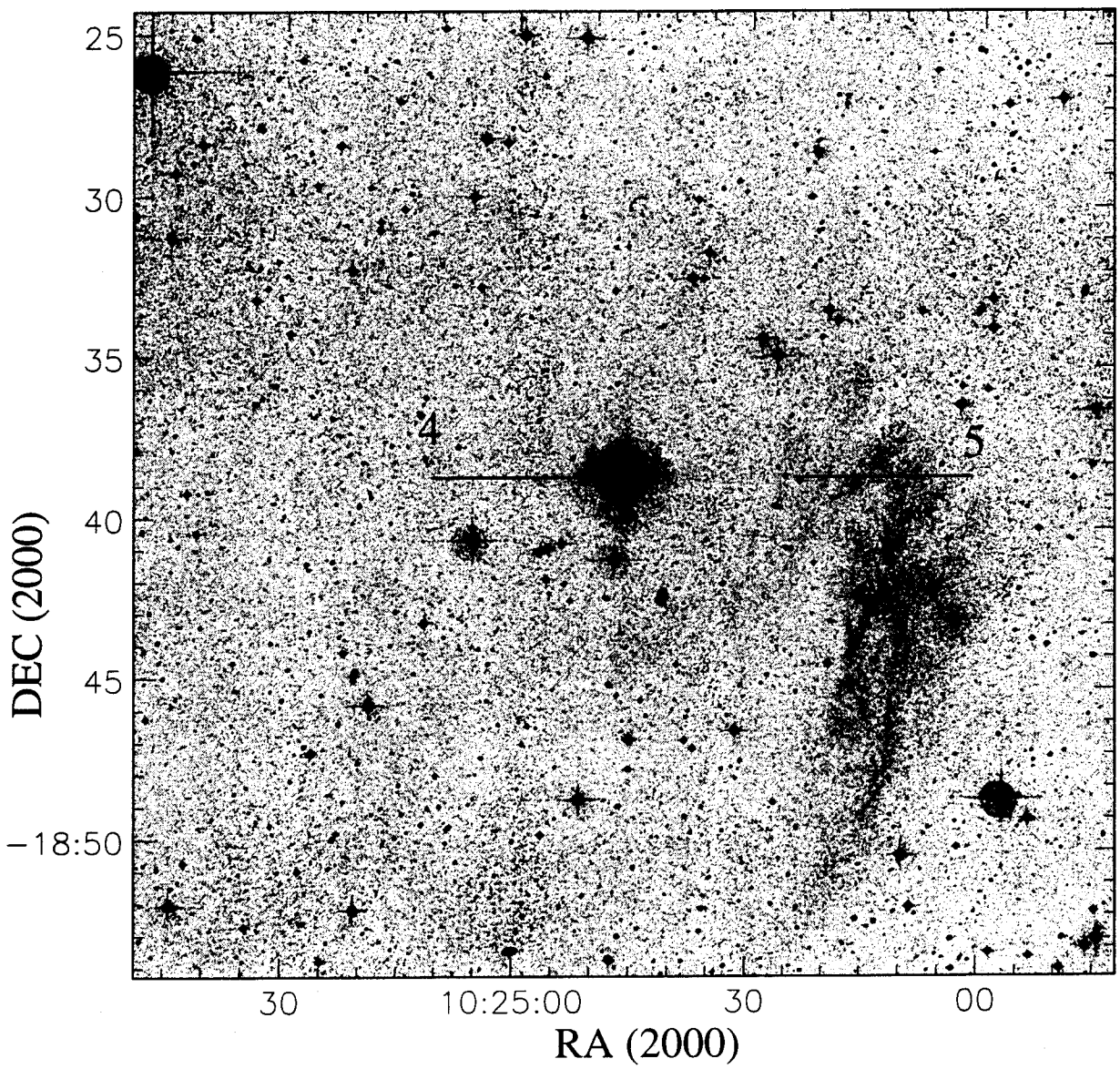
25
30
35
40
45
−18:50
DEC (2000)
4
5
30
10:25:00
30
00
RA (2000)

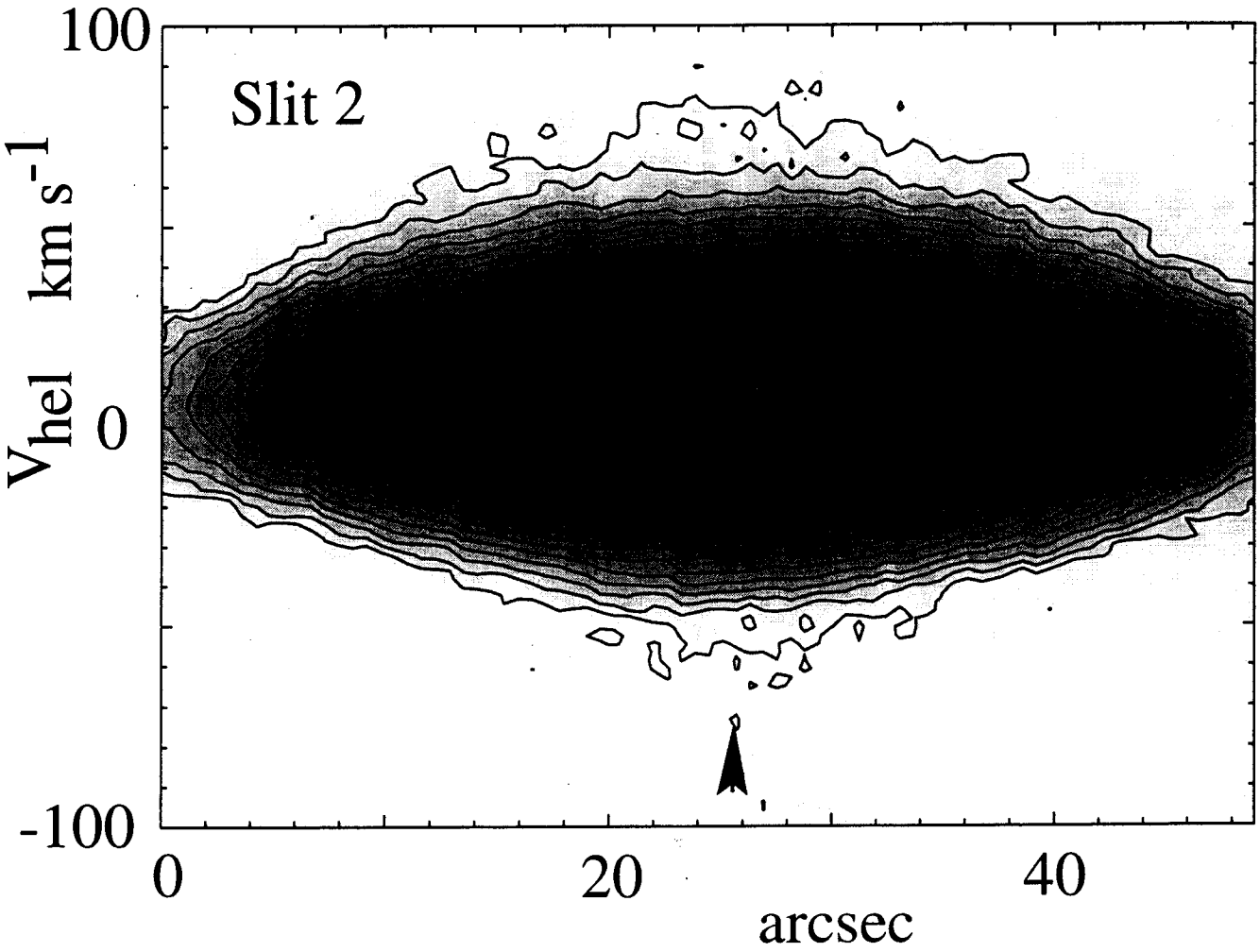
Slit 2
100
0
-100
V_{hel} km s^{-1}
0
20
40
arcsec

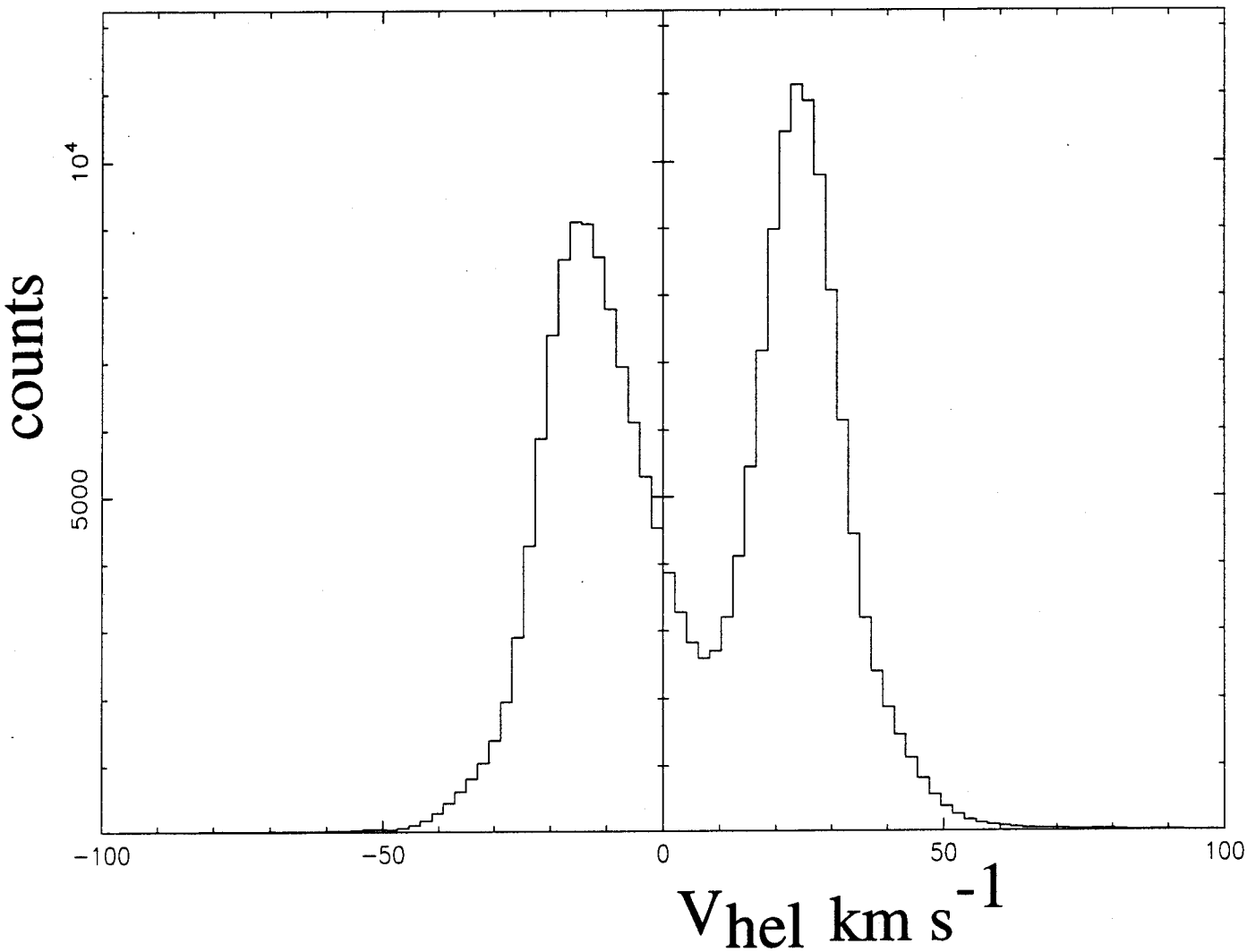
counts
10^4
5000
−100
−50
0
50
100
V_{hel} km s^{-1}

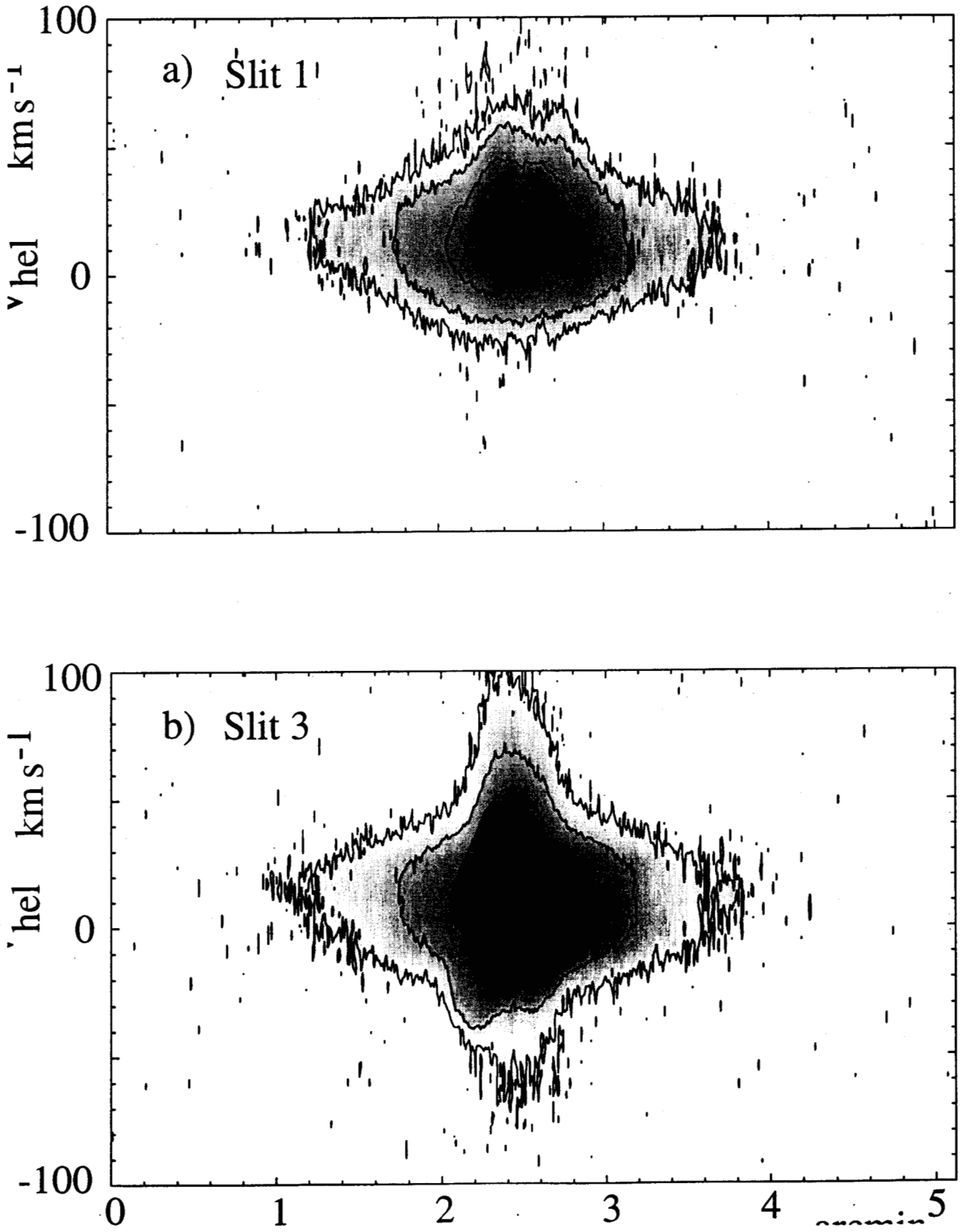
a) Slit 1
b) Slit 3
100
0
-100
v_{hel} km s^{-1}
0
1
2
3
4
5
arcmin

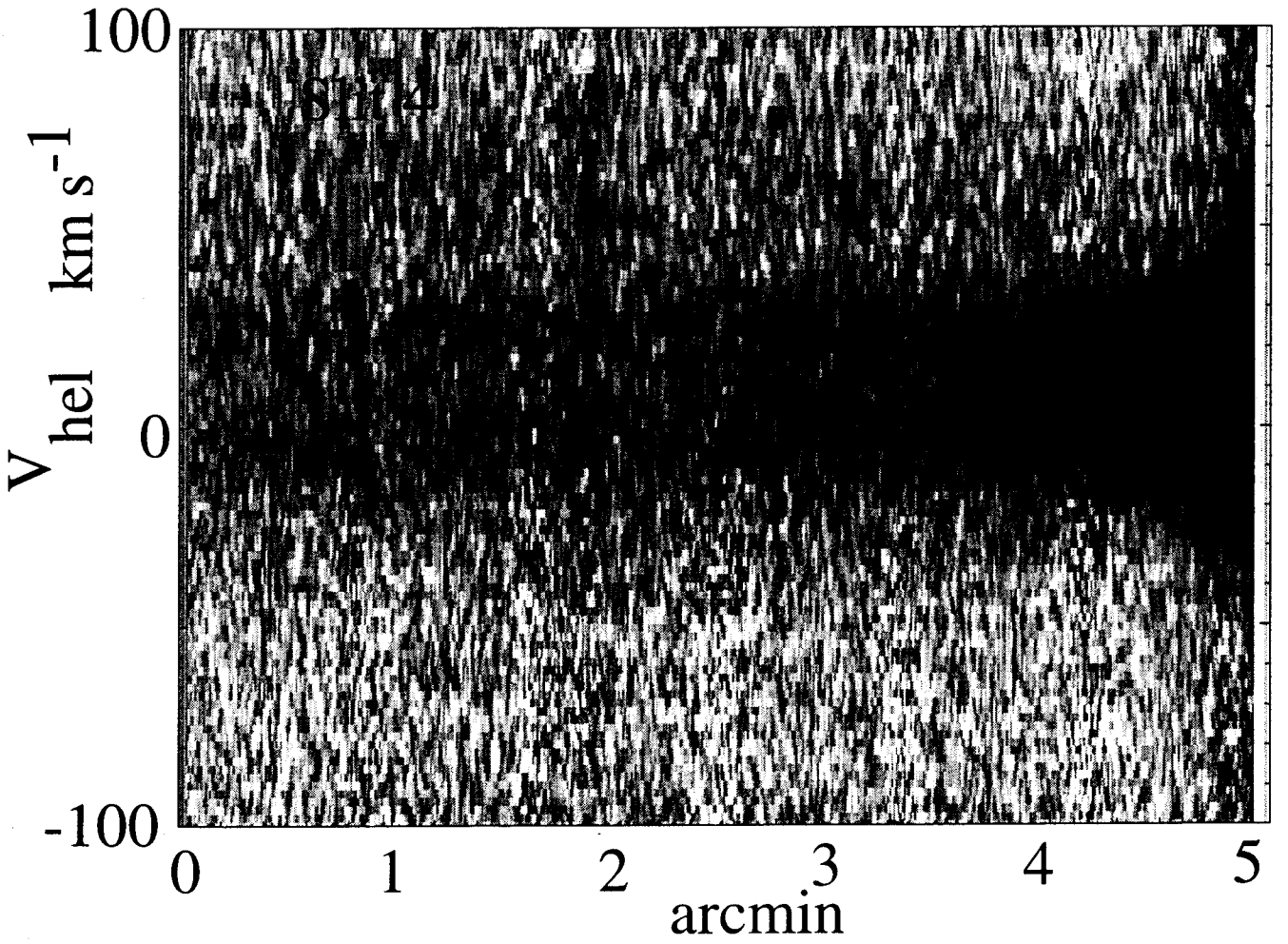
100
0
-100
V_{hel} km s^{-1}
0
1
2
3
4
5
arcmin

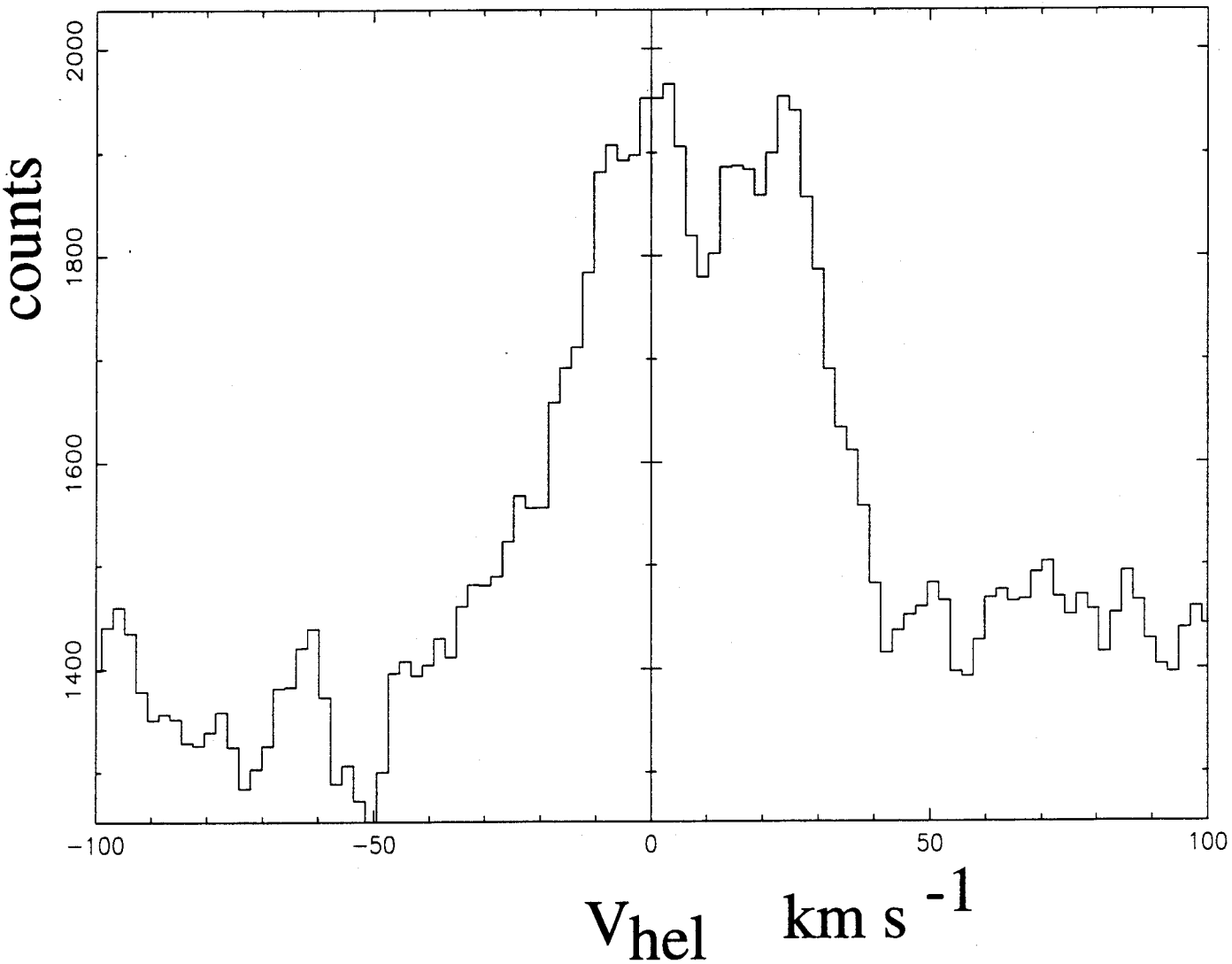
counts
2000
1800
1600
1400
−100
−50
0
50
100
V_{hel} km s $^{-1}$

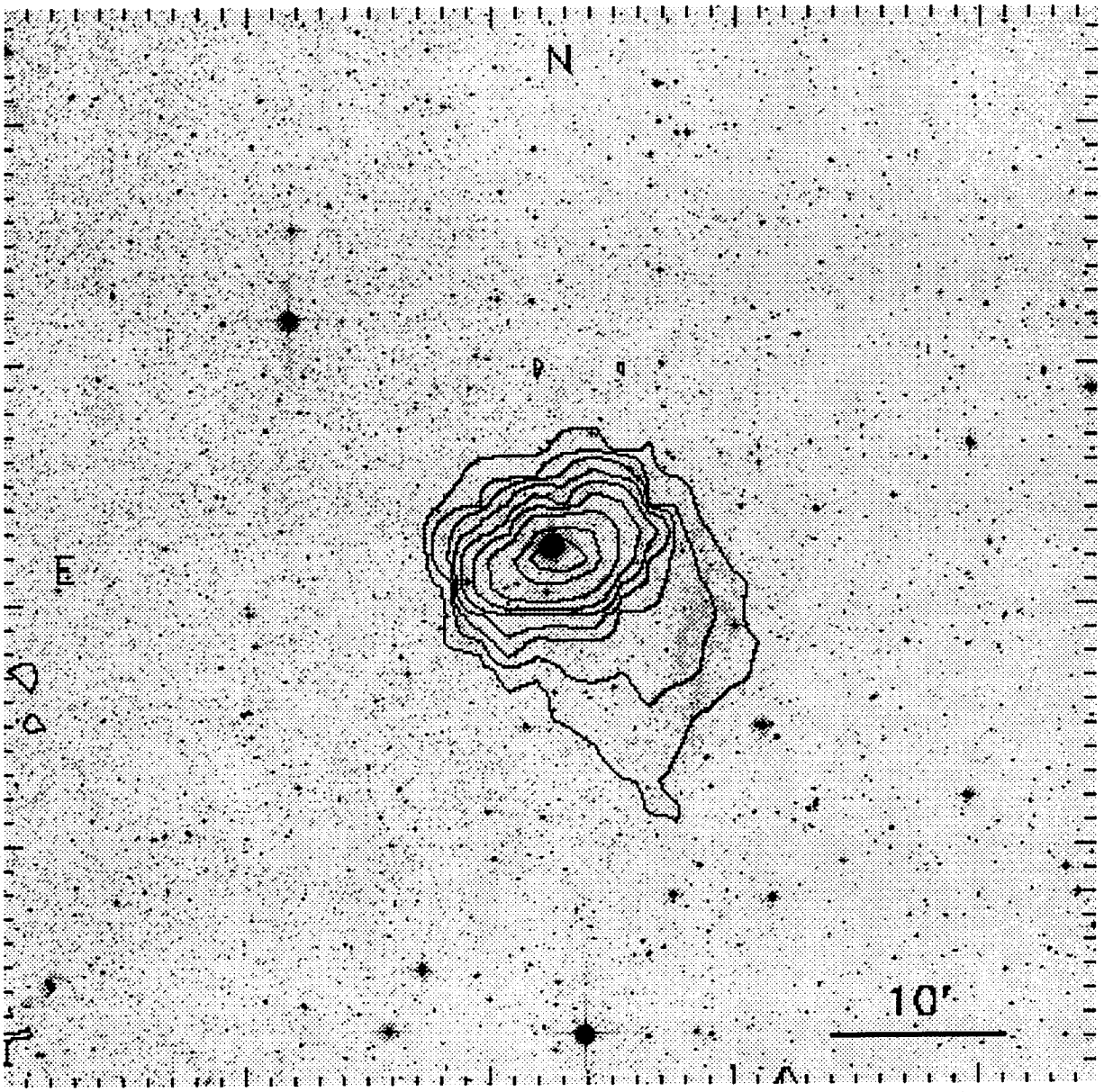
N
E
10'

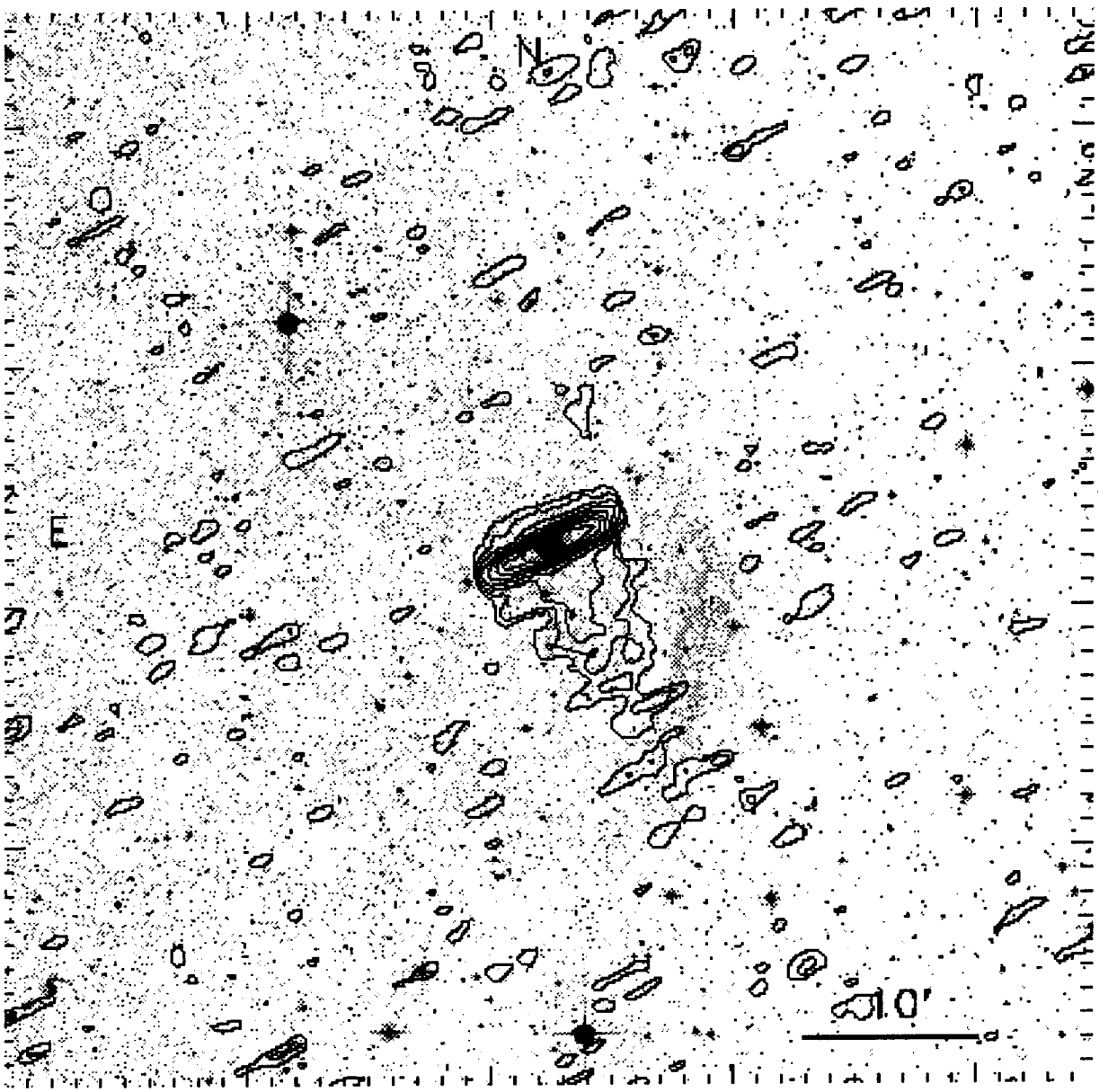
N
E
10'

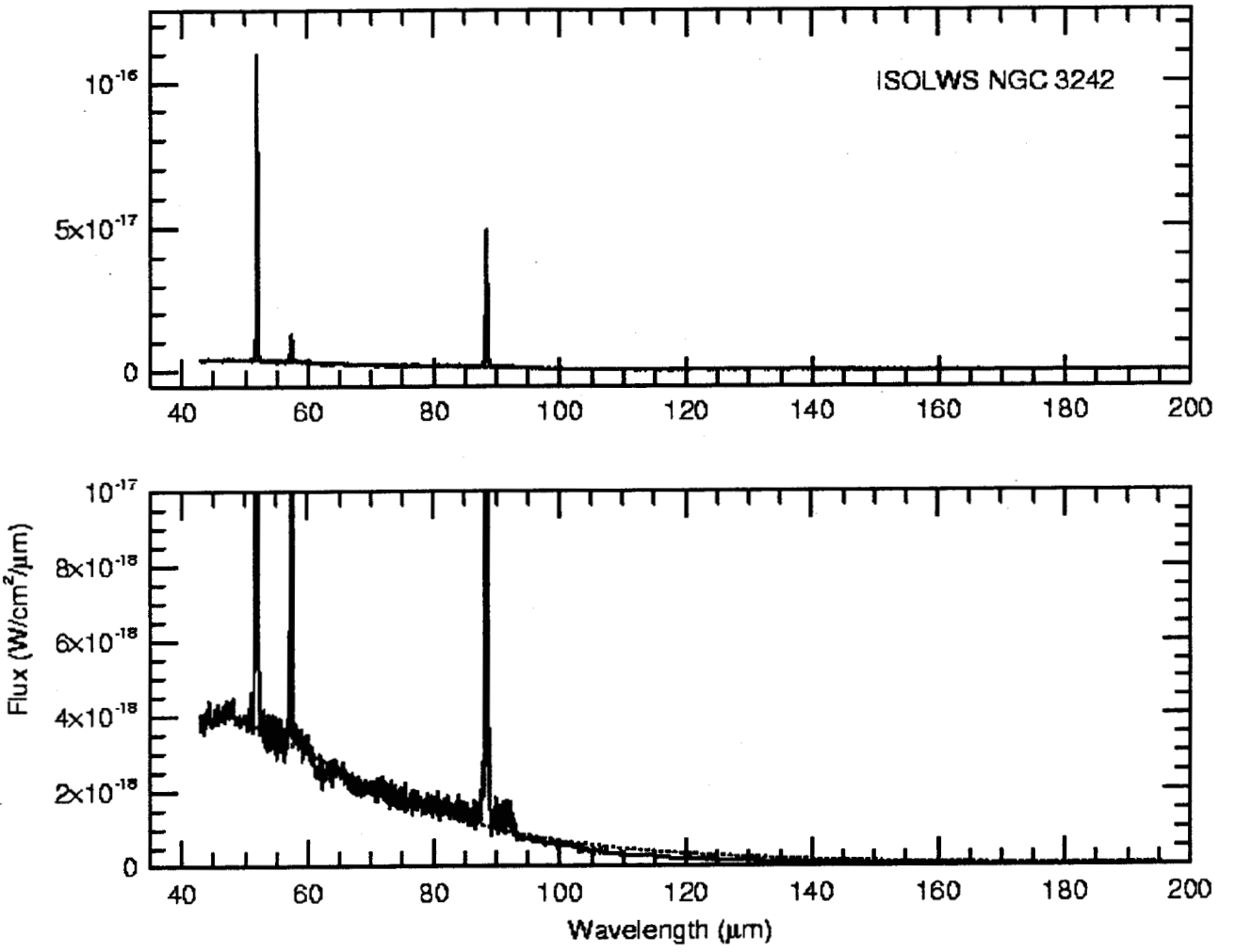
ISOLWS NGC 3242
10^{-16}
5×10^{-17}
0
40
60
80
100
120
140
160
180
200
10^{-17}
8×10^{-18}
6×10^{-18}
4×10^{-18}
2×10^{-18}
0
Flux (W/cm^2/μm)
Wavelength (μm)